Microscopic structure of high-spin vibrational excitations in superdeformed ^{190,192,194}Hg

Takashi Nakatsukasa*
Atomic Energy of Canada Limited, Chalk River Laboratories, Chalk River, Ontario K0J 1J0, Canada

Kenichi Matsuyanagi
Department of Physics, Kyoto University, Kyoto 606–01, Japan

Shoujirou Mizutori
Department of Mathematical Physics, Lund Institute of Technology, Box 118, S-22100, Lund, Sweden

Yoshifumi R. Shimizu
Department of Physics, Kyushu University, Fukuoka 812, Japan
(Received 27 November 1995)

Microscopic calculations based on the cranked shell model extended by the random-phase-approximation are performed to investigate the quadrupole and octupole correlations for excited superdeformed bands in ^{190}Hg, ^{192}Hg, and ^{194}Hg. The $K=2$ octupole vibrations are predicted to be the lowest excitation modes at zero rotational frequency. At finite frequency, however, the interplay between rotation and vibrations produces different effects depending on neutron number: The lowest octupole phonon is rotationally aligned in ^{190}Hg, is crossed by the aligned two-quasiparticle bands in ^{192}Hg, and retains the $K=2$ octupole vibrational character up to the highest frequency in ^{194}Hg. The γ vibrations are predicted to be higher in energy and less collective than the octupole vibrations. From a comparison with the experimental dynamic moments of inertia, a new interpretation of the observed excited bands invoking the $K=2$ octupole vibrations is proposed, which suggests those octupole vibrations may be prevalent in superdeformed Hg nuclei. [S0556-2813(96)05705-6]

PACS number(s): 21.10.Re, 21.60.Jz, 27.80.+w

I. INTRODUCTION

Theoretical and experimental studies of collective vibrational states built on the superdeformed (SD) yrast band are open topics of interest in the field of high-spin nuclear structure. Since the large deformation and rapid rotation of SD bands may produce a novel shell structure, we expect that surface vibrations will exhibit quite different features from those found in spherical and normal-deformed nuclei. According to our previous work [1–5], low-lying octupole vibrations are more important than quadrupole vibrations when the nuclear shape is superdeformed. Strong octupole correlations in SD states have been also suggested theoretically in Refs. [6–13]. Experimentally, octupole correlations in SD states have been suggested for ^{152}Dy [14], ^{193}Hg [15], and ^{190}Hg [16,17]. We have reported theoretical calculations corresponding to these data for ^{193}Hg [3] and ^{152}Dy [5]. In this paper, we discuss the quadrupole and octupole correlations for ^{190}Hg (which have been partially reported in Refs. [17–19]) and for the neighboring SD nuclei ^{192,194}Hg.

We have predicted the low-lying $K=2$ octupole vibrations for SD Hg isotopes ^{190,192,194}Hg ($E_x \sim 1$ MeV) [3,4]. These predictions differ from the results of generator-coordinate-method (GCM) calculations [13] in which the $K=0$ octupole state is predicted to be the lowest in SD ^{192}Hg and the excitation energies are significantly higher ($E_x \sim 2$ MeV) than in our predictions. Experimentally [17], the Routhians of the lowest octupole state decrease with the rotational frequency, for example, from $E'_x \approx 0.7$ to 0.3 MeV as $\hbar\omega_{\rm rot}$ goes from 0.25 to 0.35 MeV; therefore to compare the theoretical Routhians directly with the experimental ones, we need to calculate them at finite rotational frequency. For this purpose, the cranked shell model extended by the random-phase approximation (RPA) provides us with a powerful tool to investigate collective excitations at high angular momentum.

A great advantage of this model is its ability to take into account effects of the Coriolis coupling on the collective vibrational motions in a rapidly rotating system. Since in the normal-deformed nuclei it is known that Coriolis coupling effects are important even for the 3^- octupole states [20], one may expect strong Coriolis mixing for high-spin octupole states built on the SD yrast band. On the other hand, our previous calculations suggested weak Coriolis mixing for the lowest octupole state in ^{192}Hg [3] and ^{152}Dy [5]. This may be because the angular momentum of the octupole phonon is strongly coupled to the symmetry axis due to the large deformation of the SD shape. Generally speaking, Coriolis mixing is expected to occur more easily in nuclei with smaller deformation. However, this expectation may not hold for octupole bands in all SD nuclei because Coriolis mixing depends on the shell structure. In this paper we find a significant difference in the Coriolis mixing between an octupole band in ^{190}Hg and the other bands.

Another advantage of this model is that it gives us a unified microscopic description of collective states, weakly collective states, and noncollective two-quasiparticle excitations. A transition of the octupole vibrations into aligned two-quasiparticle bands at high spin in normal-deformed nu-

*Electronic address: nakatsukasat@cr1.aecl.ca

clei has been predicted by Vogel [21]. In Ref. [19], this transition is discussed in the context of experimental data on rare-earth and actinide nuclei, and a damping of octupole collectivity at high spin was suggested. Since similar phenomena may happen to octupole vibrations in SD states, it is important that our model describe the interplay between collective and noncollective excitations.

Recent experimental studies reveal a number of interesting features of excited SD bands in even-even Hg isotopes. In ^{190}Hg, almost constant dynamic moments of inertia, $\mathcal{J}^{(2)}$, have been observed by Crowell *et al.* [16]. Reference [17] has established the relative excitation energy of this band and confirmed the dipole character of the decay transitions into the yrast SD band. This band has been interpreted as an octupole vibrational band. Two more excited bands in ^{190}Hg have been observed recently by Wilson *et al.* [18], one of which shows a sharp rise of $\mathcal{J}^{(2)}$ at low frequency. In ^{192}Hg, Fallon *et al.* [22] have reported two excited bands which exhibit peaks in $\mathcal{J}^{(2)}$ at high frequency. In contrast with these atypical $\mathcal{J}^{(2)}$ behaviors, two excited bands in ^{194}Hg originally observed by Riley *et al.* [23] and extended by Cederwall *et al.* [24] show a smooth increase with rotational frequency. We show in this paper that this $\mathcal{J}^{(2)}$ behavior can be explained with a single theoretical model which microscopically takes into account shape vibrations and the Coriolis force.

The purpose of this paper is to present the RPA method based on the cranked shell model and its ability to describe a variety of nuclear properties including shape vibrations at large deformation and high spin. We propose a plausible interpretation for the microscopic structure of excited SD bands in ^{190,192,194}Hg, and show that octupole bands may be more prevalent than expected in these SD nuclei. Section II presents a description of the model, in which we stress our improvements to the cranked Nilsson potential and to the coupled RPA method in a rotating system. Section III presents details of the calculation in which the pairing and effective interactions are discussed. The results for the excited SD ^{190}Hg, ^{192}Hg, and ^{194}Hg are presented in Sec. IV, and compared with the experimental data in Sec. V. The conclusions are summarized in Sec. VI.

II. THEORETICAL FRAMEWORK

The theory of the cranked shell model extended by the random-phase approximation (RPA) was first developed by Marshalek [25] and has been applied to high-spin β and γ vibrational bands [26–28] and to octupole bands [29,1–5]. Since this theory is suitable for describing the collective vibrations built on deformed high-spin states, it is very useful for investigating vibrational motion built on the SD yrast band.

A. Cranked Nilsson potential with the local Galilean invariance

We start with a rotating mean field with a rotational frequency $\omega_{\rm rot}$ described by

$$h_{\rm s.p.}=h_{\rm Nilsson}+\Gamma_{\rm pair}-\omega_{\rm rot}J_x+h_{\rm add}, \tag{2.1}$$

where $h_{\rm Nilsson}$ is a standard Nilsson potential defined in single-stretched coordinates $r_i'=(\omega_i/\omega_0)^{1/2}r_i$ and $p_i'=(\omega_0/\omega_i)^{1/2}p_i$ $(i=x,y,z)$,

$$h_{\rm Nilsson}=\sum_{i=x,y,z}\left(\frac{\omega_i}{\omega_0}\right)\left(\frac{p_i'^{\,2}}{2M}+\frac{M\omega_0^2}{2}r_i'^{\,2}\right)+v_{ll}(\boldsymbol{l}'^{\,2}-\langle\boldsymbol{l}'^{\,2}\rangle_N)+v_{ls}\boldsymbol{l}'\cdot\mathbf{s}, \tag{2.2}$$

where $\boldsymbol{l}'=\mathbf{r}'\times\mathbf{p}'$. The pairing field $\Gamma_{\rm pair}$ is defined by

$$\Gamma_{\rm pair}=-\sum_{\tau=n,p}\Delta_\tau(P_\tau^\dagger+P_\tau)-\sum_{\tau=n,p}\lambda_\tau N_\tau, \tag{2.3}$$

where $P_\tau=\Sigma_{k\in\tau,k>0}c_k\bar{c}_k$ and $N_\tau=\Sigma_{k\in\tau}c_k^\dagger c_k$ are the monopole-pairing and number operators, respectively. In Sec. III A, we discuss the details of the pairing field used in the calculations.

A standard cranked Nilsson potential has the disadvantage that it overestimates the moments of inertia compared to a Woods-Saxon potential. This problem comes from the spurious velocity dependence associated with the $\boldsymbol{l}^2$ term in the Nilsson potential which is absent for Woods-Saxon potential. If the mean-field potential is velocity independent, the local velocity distribution in the rotating nucleus remains isotropic in velocity space, which means that the flow pattern becomes the same as for a rigid-body rotation [30]. However, in the cranked Nilsson potential, this isotropy of the velocity distribution is significantly broken due to the $\boldsymbol{l}^2$ term. Thus the Coriolis force introduces a spurious flow in the rotating coordinate system, proportional to the rotational frequency. This spurious effect can be compensated by an additional term that restores the local Galilean invariance. This additional term is obtained by substituting (the local Galilean transformation)

$$\mathbf{p}\rightarrow\mathbf{p}-M(\boldsymbol{\omega}_{\rm rot}\times\mathbf{r}), \tag{2.4}$$

in the $\boldsymbol{ls}$ and $\boldsymbol{l}^2$ terms of the Nilsson potential. This prescription was suggested by Bohr and Mottelson [30], and developed by Kinouchi [31]. For a momentum-dependent potential $V(\mathbf{r},\mathbf{p})$,

$$V(\mathbf{r},\mathbf{p})+h_{\rm add}=V(\mathbf{r},\mathbf{p}-M(\boldsymbol{\omega}_{\rm rot}\times\mathbf{r})) \tag{2.5}$$

$$\approx V(\mathbf{r},\mathbf{p})-\omega_{\rm rot}M\left(y\frac{\partial}{\partial p_z}-z\frac{\partial}{\partial p_y}\right)V(\mathbf{r},\mathbf{p}) \tag{2.6}$$

$$=V(\mathbf{r},\mathbf{p})+\frac{i}{\hbar}\omega_{\rm rot}M(y[z,V]-z[y,V]), \tag{2.7}$$

where we assume uniform rotation around the x axis, $\omega_{\rm rot}=(\omega_{\rm rot},0,0)$. Following this prescription, the additional term $h_{\rm add}$ in Eq. (2.1) is obtained for the Nilsson potential (2.2),

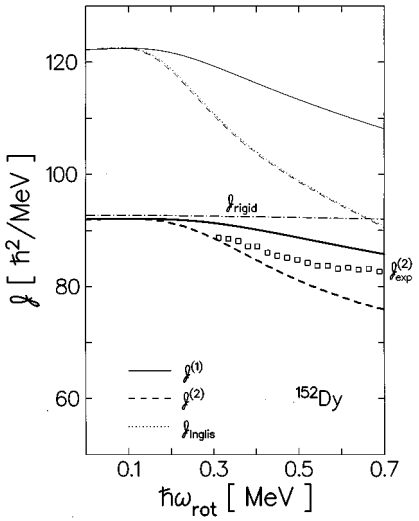

FIG. 1. Kinematic (solid lines) and dynamic (dashed lines) moments of inertia for SD ^{152}Dy calculated in the cranked Nilsson Hamiltonian with (thick lines) and without (thin lines) the additional term $h_{\rm add}$ in Eq. (2.8). The rigid-body and the Inglis moments of inertia are shown by dash-dotted and dotted lines, respectively. The parameters used in the calculation are the same as those used in Ref. [5] and pairing correlations are neglected. Symbols are experimental $\mathscr{J}^{(2)}$ taken from Ref. [14].

$$h_{\rm add}=-\frac{\omega_{\rm rot}}{\sqrt{\omega_y\omega_z}}\left\{v_{ll}\left[2M\omega_0\mathbf{r}'^2-\hbar\left(N_{\rm osc}+\frac{3}{2}\right)\right]l'_x + v_{ls}M\omega_0[\mathbf{r}'^2 s_x-r'_x(\mathbf{r}'\cdot\mathbf{s})]\right\}. \tag{2.8}$$

Note that the term proportional to $(N_{\rm osc}+3/2)$ in Eq. (2.8) comes from the velocity dependence of $\langle \boldsymbol{l}'^2\rangle_N$ in Eq. (2.2). This result, Eq. (2.8), has been applied to the SD bands in ^{152}Dy [5] where the single-particle Routhians were found to be very similar to those obtained by using the Woods-Saxon potential. In Fig. 1, moments of inertia for SD ^{152}Dy calculated with and without the additional term (2.8) are displayed. Since the effects of the mixing among the major oscillator shells $N_{\rm osc}$ are neglected in calculating our Routhians, kinematic ($\mathscr{J}^{(1)}$) and dynamic ($\mathscr{J}^{(2)}$) moments of inertia are obtained by adding the contributions of the $N_{\rm osc}$-mixing effects to the values calculated without them:

$$\mathscr{J}^{(1)}=\frac{\langle J_x\rangle}{\omega_{\rm rot}}+\frac{1}{\omega_{\rm rot}}\int_0^{\omega_{\rm rot}}\Delta\mathscr{J}_{\rm Inglis}(\omega)d\omega \approx \frac{\langle J_x\rangle}{\omega_{\rm rot}}+\Delta\mathscr{J}_{\rm Inglis}, \tag{2.9}$$

$$\mathscr{J}^{(2)}=\frac{d\langle J_x\rangle}{d\omega_{\rm rot}}+\Delta\mathscr{J}_{\rm Inglis}, \tag{2.10}$$

$$\Delta\mathscr{J}_{\rm Inglis}=\mathscr{J}_{\rm Inglis}-\mathscr{J}^{\Delta N=0}_{\rm Inglis} =2\sum_{n(\Delta N=2)}\frac{|\langle n|J_x|0\rangle|^2}{E_n-E_0}, \tag{2.11}$$

where $\Delta\mathscr{J}_{\rm Inglis}$ is difference between the Inglis moments of inertia with and without the $\Delta N_{\rm osc}=2$ contributions [32]. $\Delta\mathscr{J}_{\rm Inglis}(\omega)$ turned out to be approximately constant against frequency ω and this was used in the last step of Eq. (2.9). The $\mathscr{J}^{(1)}$ and $\mathscr{J}^{(2)}$ values calculated with the additional term are very close to the rigid-body value at low frequency, which means that the spurious effects of the $\boldsymbol{l}^2$ term have been removed. Note that the abscissa of Fig. 1 corresponds to the ''bare'' rotational frequency without renormalization. The drastic reduction of $\mathscr{J}^{(1)}$ and $\mathscr{J}^{(2)}$ at high frequency is corrected by the additional term, and this is seen to be important in reproducing the experimental $\mathscr{J}^{(2)}$ behavior of the yrast SD band.

B. RPA in the rotating frame

The residual interactions are assumed to be in a separable form

$$H_{\rm int}=-\frac{1}{2}\sum_{\rho,\alpha}\chi_\rho R^\alpha_\rho R^\alpha_\rho, \tag{2.12}$$

where R^α_ρ are one-body Hermitian operators, and χ_ρ are coupling strengths. The indices α indicate the signature quantum numbers ($\alpha=0,1$) and ρ specifies other modes. In this paper, we take as R^α_ρ the monopole pairing and the quadrupole operators for positive-parity states, and the octupole and the isovector dipole operators for negative-parity states [see Eq. (3.5)]. Since the K quantum number is not conserved at finite rotational frequency, it is more convenient to make the multipole operators have good signature quantum numbers. In general, the Hermitian multipole (spin-independent) operators with good signature quantum numbers are constructed by

$$Q^\alpha_{\lambda K}=\frac{i^{\lambda+\alpha+K}}{\sqrt{2(1+\delta_{K0})}}[r^\lambda Y_{\lambda K}+(-)^{\lambda+\alpha}r^\lambda Y_{\lambda -K}], \tag{2.13}$$

with $K\geqslant 0$, where the spherical-harmonic functions $Y_{\lambda K}$ are defined with respect to the symmetry (z) axis. All multipole operators are defined in doubly stretched coordinates $[r''_i=(\omega_i/\omega_0)r_i]$, which can be regarded as an improved version of the conventional multipole interaction. Sakamoto and Kishimoto [33] have shown that at the limit of the harmonic-oscillator potential (at $\omega_{\rm rot}=0$), it guarantees nuclear self-consistency [30], restoration of the symmetry broken in the mean field, and separation of the spurious solutions. The coupling strengths χ_ρ should be determined by the self-consistency condition between the density distribution and the single-particle potential (see Sec. III B for details).

To describe vibrational excitations in the RPA theory, we must define the *quasiparticle vacuum* on which the vibrations are built. The observed moments of inertia, $\mathscr{J}^{(2)}$, of the yrast SD bands smoothly increase in the $A=190$ region, which suggests that the internal structure also smoothly changes as a function of the frequency $\omega_{\rm rot}$. Therefore the *adiabatic representation*, in which the quasiparticle operators are always defined with respect to the yrast state $|\omega_{\rm rot}\rangle$, is considered to be appropriate in this work.

In terms of quasiparticles, the Hamiltonian of Eq. (2.1) can be diagonalized (by the general Bogoliubov transformation) as

$$h_{\text{s.p.}} = \text{const} + \sum_{\mu} (E_{\mu} a_{\mu}^{\dagger} a_{\mu}) + \sum_{\mu} (E_{\bar{\mu}} a_{\bar{\mu}}^{\dagger} a_{\bar{\mu}}), \quad (2.14)$$

with

$$a_{\mu} |\omega_{\text{rot}}\rangle = a_{\bar{\mu}} |\omega_{\text{rot}}\rangle = 0, \quad (2.15)$$

where $(a_{\mu}^{\dagger}, a_{\bar{\mu}}^{\dagger})$ represent the quasiparticles with signature $\alpha = (1/2, -1/2)$, respectively. The excitation operators of the RPA normal modes $X_n^{\alpha\dagger}$ $(\alpha = 0,1)$ are defined by

$$X_n^{0\dagger} = \sum_{\mu\nu} \{\psi_n^0(\mu\bar{\nu}) a_{\mu}^{\dagger} a_{\bar{\nu}}^{\dagger} + \varphi_n^0(\mu\bar{\nu}) a_{\bar{\nu}} a_{\mu}\}, \quad (2.16)$$

$$X_n^{1\dagger} = \sum_{\mu<\nu} \{\psi_n^1(\mu\nu) a_{\mu}^{\dagger} a_{\nu}^{\dagger} + \varphi_n^1(\mu\nu) a_{\nu} a_{\mu}\} + \sum_{\mu<\nu} \{\psi_n^1(\bar{\mu}\bar{\nu}) a_{\bar{\mu}}^{\dagger} a_{\bar{\nu}}^{\dagger} + \varphi_n^1(\bar{\mu}\bar{\nu}) a_{\bar{\nu}} a_{\bar{\mu}}\}, \quad (2.17)$$

where indices n specify excited states and $\psi_n^{\alpha}(\mu\nu)$ $[\varphi_n^{\alpha}(\mu\nu)]$ are the RPA forward [backward] amplitudes. Quasiparticle-scattering terms such as $a_{\mu}^{\dagger} a_{\nu}$ are regarded as higher-order terms in the boson-expansion theory and are neglected in the RPA.[1]

The equation of motion and the normalization condition in the RPA theory,

$$[h_{\text{s.p.}} + H_{\text{int}}, X_n^{\alpha\dagger}]_{\text{RPA}} = \hbar\Omega_n^{\alpha} X_n^{\alpha\dagger}, \quad (2.18)$$

$$[X_n^{\alpha}, X_{n'}^{\alpha\,\dagger}]_{\text{RPA}} = \delta_{nn'}, \quad (2.19)$$

are solved with the following multidimensional response functions:

$$S_{\rho\rho'}^{\alpha}(\Omega) = \sum_{\gamma\delta} \left\{ \frac{R_{\rho}^{\alpha}(\gamma\delta)^* R_{\rho'}^{\alpha}(\gamma\delta)}{E_{\gamma} + E_{\delta} - \hbar\Omega} + \frac{R_{\rho}^{\alpha}(\gamma\delta) R_{\rho'}^{\alpha}(\gamma\delta)^*}{E_{\gamma} + E_{\delta} + \hbar\Omega} \right\}, \quad (2.20)$$

where $(\gamma\delta) = (\mu\bar{\nu})$ for $\alpha = 0$ states, and $(\gamma\delta) = (\mu < \nu), (\bar{\mu} < \bar{\nu})$ for $\alpha = 1$ states. The two-quasiparticle matrix elements $R_{\rho}^{\alpha}(\gamma\delta)$ are defined by $R_{\rho}^{\alpha}(\gamma\delta) \equiv \langle\omega_{\text{rot}}| a_{\delta} a_{\gamma} R_{\rho}^{\alpha} |\omega_{\text{rot}}\rangle$. Let us denote the transition matrix elements between the RPA excited states $|n\rangle$ and the yrast state as

$$\begin{aligned} t_{\rho}^{\alpha}(n) &\equiv t_n[R_{\rho}^{\alpha}] \equiv \langle\omega_{\text{rot}}| R_{\rho}^{\alpha} |n\rangle \\ &= \langle\omega_{\text{rot}}| [R_{\rho}^{\alpha}, X_n^{\alpha\dagger}] |\omega_{\text{rot}}\rangle \\ &= [R_{\rho}^{\alpha}, X_n^{\alpha\dagger}]_{\text{RPA}}. \end{aligned} \quad (2.21)$$

Then, the equation of motion (2.18) is equivalent to

$$t_{\rho}^{\alpha}(n) = \sum_{\rho'} \chi_{\rho}^{\alpha} S_{\rho\rho'}^{\alpha}(\Omega) t_{\rho'}^{\alpha}(n). \quad (2.22)$$

RPA solutions (eigenenergies) $\hbar\Omega_n$ are obtained by solving the equation

$$\det\left(S_{\rho\rho'}^{\alpha}(\Omega) - \frac{1}{\chi_{\rho}} \delta_{\rho\rho'} \right) = 0, \quad (2.23)$$

which corresponds to the condition that Eq. (2.22) have a nontrivial solution $[t_{\rho}^{\alpha}(n) \neq 0]$. Each RPA eigenstate is characterized by the corresponding forward and backward amplitudes which are calculated as

$$\psi_n^{\alpha}(\gamma\delta) = \frac{\Sigma_{\rho} \chi_{\rho}^{\alpha} t_{\rho}^{\alpha}(n) R_{\rho}^{\alpha}(\gamma\delta)}{E_{\gamma} + E_{\delta} - \hbar\Omega_n}, \quad (2.24)$$

$$\varphi_n^{\alpha}(\gamma\delta) = \frac{-\Sigma_{\rho} \chi_{\rho}^{\alpha} t_{\rho}^{\alpha}(n) R_{\rho}^{\alpha}(\gamma\delta)^*}{E_{\gamma} + E_{\delta} + \hbar\Omega_n}, \quad (2.25)$$

and satisfies the normalization condition (2.19). The transition matrix elements $\langle\omega_{\text{rot}}|Q|n\rangle$ of any one-body operator Q can be expressed in terms of these amplitudes ψ_n and φ_n:

$$\begin{aligned} t_n[Q] &\equiv \langle\omega_{\text{rot}}|Q|n\rangle \\ &= \sum_{\gamma\delta} \{Q(\gamma\delta)^* \psi_n(\gamma\delta) - Q(\gamma\delta) \varphi_n(\gamma\delta)\}. \end{aligned} \quad (2.26)$$

The phase relation between the matrix elements $Q(\gamma\delta)$ and the amplitudes $(\psi_n(\gamma\delta), \varphi_n(\gamma\delta))$ is very important, because it determines whether the transition matrix element $t_n[Q]$ is coherently enhanced or canceled out after the summation in Eq. (2.26). For instance, a collective quadrupole vibrational state has a favorable phase relation for the quadrupole operators. Therefore, it gives large matrix elements for the $E2$ operators, while for the $M1$ operators, the contributions are normally canceled out after the summation.

Finally we obtain a diagonal form of the total Hamiltonian in the rotating frame by means of the RPA theory,

$$H' = h_{\text{s.p.}} + H_{\text{int}} \approx E_0' + \sum_{n,\alpha} \hbar\Omega_n^{\alpha} X_n^{\alpha\dagger} X_n^{\alpha}, \quad (2.27)$$

where E_0' corresponds to the Routhians for the yrast configuration. Since we are interested in the relative excitation energy between excited states and the yrast state, E_0' need not be explicitly calculated. It is worth noting that since the effect of the cranking term on the quasiparticles depends on rotational frequency, the effects of Coriolis coupling on the RPA eigenstates are automatically taken into account.

III. DETAILS OF CALCULATIONS

A. Mean-field parameters and the improved quasiparticle Routhians

We adopt standard values for the parameters v_{ll} and v_{ls} [34] and use different values of the oscillator frequency ω_0

[1] In the following, the notation $[A,B]_{\text{RPA}}$ means that we neglect these higher-order terms in calculating the commutator between A and B.

for neutrons and protons in the Nilsson potential (2.2) in order to ensure equal root-mean-square radii [35]:

$$\omega_0 \rightarrow \begin{cases} \left(\frac{2N}{A}\right)^{1/3} \omega_0 & \text{for neutrons,} \\ \left(\frac{2Z}{A}\right)^{1/3} \omega_0 & \text{for protons,} \end{cases} \tag{3.1}$$

where $\hbar\omega_0 = 41A^{-1/3}$ MeV.

The quadrupole deformation ϵ is determined by minimizing the total Routhian surface (TRS), and the strength for the monopole pairing interaction G is taken from the prescription of Ref. [36] with the average pairing gap $\tilde{\Delta} = 12A^{-1/2}$ MeV and the cutoff parameter of the pairing model space $\Lambda = 1.2\hbar\omega_0$. In principle the pairing gaps (Δ_n, Δ_p) and the chemical potentials (λ_n, λ_p) should be calculated self-consistently satisfying the usual BCS conditions at each rotational frequency:

$$G_\tau \langle \omega_{\rm rot} | P_\tau | \omega_{\rm rot} \rangle = \Delta_\tau, \tag{3.2}$$

$$\langle \omega_{\rm rot} | N_\tau | \omega_{\rm rot} \rangle = N(Z), \tag{3.3}$$

with $\tau = (n,p)$. However, the mean-field treatment of the pairing interaction predicts a sudden collapse of the proton pairing gap at $\hbar\omega_{\rm rot} \approx 0.3$ MeV and of the neutron gap at $\hbar\omega_{\rm rot} \approx 0.5$ MeV. This transition causes a singular behavior in the moments of inertia which is inconsistent with experimental observations. It arises from the poor treatment of number conservation, and such sudden transitions should not occur in a finite system like the nucleus. In this paper we have therefore adopted the following phenomenological prescription for the pairing correlations at finite frequency [37]:

$$\Delta_\tau(\omega) = \begin{cases} \Delta_\tau(0)\left[1 - \frac{1}{2}\left(\frac{\omega}{\omega_c}\right)^2\right] & \text{for } \omega < \omega_c, \\ \frac{1}{2}\Delta_\tau(0)\left(\frac{\omega_c}{\omega}\right)^2 & \text{for } \omega > \omega_c. \end{cases} \tag{3.4}$$

The chemical potentials are calculated with Eq. (3.3) at each rotational frequency. The parameters $\Delta(0) = 0.8$ (0.6) MeV and $\hbar\omega_c = 0.5$ (0.3) MeV for neutrons (protons) are used in common for ^{190,192,194}Hg.

The quadrupole deformation $\epsilon = 0.44$ is used in the calculations. For simplicity, we assume the deformation to be constant with rotational frequency, and neglect hexadecapole deformation.[2] The equilibrium deformation and pairing gaps have been determined at $\omega_{\rm rot} = 0$, with the truncated pairing model space $\Lambda = 1.2\hbar\omega_0$. Then, the pairing force strengths G_τ are adjusted so as to reproduce the pairing gap of Eq. (3.4) in the whole model space.

The experiments [16,17] have reported a sharp rise of $\mathcal{J}^{(2)}$ moments of inertia for the yrast SD band in ^{190}Hg at $\hbar\omega_{\rm rot} \approx 0.4$ MeV. This rise was reproduced in the cranked Woods-Saxon calculations [38] and results from a crossing between the yrast band and the aligned $\nu(j_{15/2})^2$ band; however, the predicted crossing frequency was lower ($\hbar\omega_{\rm rot} \approx 0.3$ MeV) than in the experiment. Our Nilsson potential without the additional term (2.8) indicates the same disagreement. In order to demonstrate the effects of the term $h_{\rm add}$ on the Routhians, we present in Fig. 2 the quasiparticle Routhians for ^{190}Hg with $h_{\rm add}$, without $h_{\rm add}$, and for the standard Woods-Saxon potential ($\beta_2 = 0.465$, $\beta_4 = 0.055$). By including $h_{\rm add}$, the correct frequency is reproduced. This term affects the proton Routhians: For example, the alignment of the intruder $\pi j_{15/2}(\alpha = -1/2)$ orbit is predicted to be $i \approx 6.5\hbar$ without $h_{\rm add}$ and this orbit becomes the lowest at $\hbar\omega_{\rm rot} \geq 0.37$ MeV. The alignment is significantly reduced ($i \approx 4\hbar$) with $h_{\rm add}$. The behavior of high-N intruder orbits in the proton Routhians is similar to that in the Woods-Saxon potential. It is worth noting that the conventional renormalization in the Nilsson potential scales the rotational frequency for all orbits, while Eq. (2.8) renormalizes alignment in a different way depending on the spurious effect on each orbit.

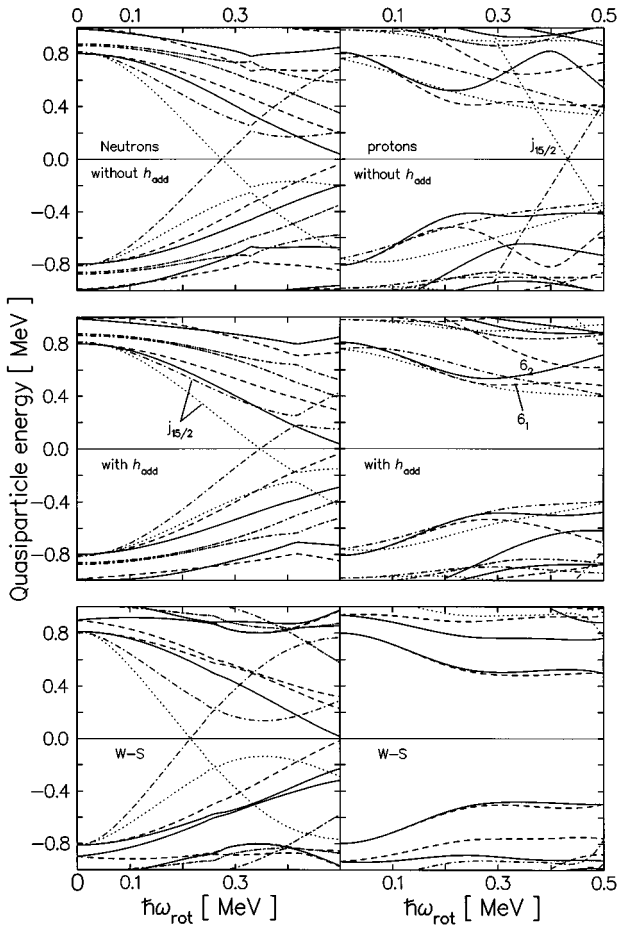

FIG. 2. Quasiparticle Routhians for neutrons (left) and protons (right) in ^{190}Hg. The top parts show the Routhians in the Nilsson potential without the additional term $h_{\rm add}$, the middle for those with $h_{\rm add}$, and the bottom for those in the Woods-Saxon potential with the ''universal'' parameters. Solid, dashed, dotted, and dash-dotted lines correspond to quasiparticles with $(\pi,\alpha) = (+,-1/2)$, $(+,1/2)$, $(-,-1/2)$, and $(-,1/2)$, respectively. See text for details.

[2]Possible errors caused by this simplification will not affect our conclusion because the property of collective RPA solutions under consideration may be insensitive to such details (see also discussions in Sec. IV A).

B. Residual interactions and the RPA

We adopt the following operators as R_ρ^α in the residual interactions (2.12):

$$P_+ \quad P_- \quad Q_{20}^0 \quad Q_{21}^\alpha \quad Q_{22}^\alpha \text{ for } \pi=+,$$
$$Q_{30}^1 \quad Q_{31}^\alpha \quad Q_{32}^\alpha \quad Q_{33}^\alpha \quad \tilde{\tau}_3 Q_{10}^1 \quad \tilde{\tau}_3 Q_{11}^\alpha \text{ for } \pi=-, \tag{3.5}$$

where $\tilde{\tau}_3=\tau_3-(N-Z)/A$ which is needed to guarantee the translational invariance. Here, the operators $Q_{\lambda K}^\alpha$ are defined by Eq. (2.13) in the doubly stretched coordinates, and $P_\pm$ are defined by

$$P_+=\frac{1}{\sqrt{2}}(\tilde{P}+\tilde{P}^\dagger), \tag{3.6}$$

$$P_-=\frac{i}{\sqrt{2}}(\tilde{P}-\tilde{P}^\dagger), \tag{3.7}$$

where $\tilde{P}=P-\langle\omega_{\rm rot}|P|\omega_{\rm rot}\rangle$. Note that the $K=0$ quadrupole (octupole) operator Q_{20} (Q_{30}) has a unique signature $\alpha=0$ ($\alpha=1$), which corresponds to the fact that $K=0$ bands have no signature partners.

Since we use the different oscillator frequency ω_0 for neutrons and protons in the Nilsson potential [see Eq. (3.1)], we use the following modified doubly stretched multipole operators for the isoscalar channels:

$$Q_{\lambda K}^\alpha \rightarrow \begin{cases} \left(\frac{2N}{A}\right)^{2/3} Q_{\lambda K}^\alpha & \text{for neutrons,} \\ \left(\frac{2Z}{A}\right)^{2/3} Q_{\lambda K}^\alpha & \text{for protons.} \end{cases} \tag{3.8}$$

This was originally proposed by Baranger and Kumar [35] for quadrupole operators. Recently Sakamoto [39] has generalized it for an arbitrary multipole operator and proved that by means of this scaling the translational symmetry is restored in the limit of the harmonic-oscillator potential. In addition, for the collective RPA solutions this treatment makes the transition amplitudes of the electric operators approximately Z/A of those of the mass operators, in the same way as in the case of the static quadrupole moments [28].

We use the pairing force strengths G_τ reproducing the pairing gaps of Eq. (3.4). For the isovector dipole coupling strengths, we adopt the standard values in Ref. [30],

$$\chi_{1K}=-\frac{\pi V_1}{A\langle(r^2)''\rangle_0}, \tag{3.9}$$

with $A\langle(r^2)''\rangle_0=\langle\Sigma_k^A(r_k^2)''\rangle_0$ and $V_1=130$ MeV. The self-consistent values for the coupling strengths $\chi_{\lambda K}$ of the isoscalar quadrupole and octupole interactions can be obtained for the case of the anisotropic harmonic-oscillator potential [33,39]:

$$\chi_{2K}^{\rm HO}=\frac{4\pi M\omega_0^2}{5A\langle(r^2)''\rangle}, \tag{3.10}$$

$$\chi_{3K}^{\rm HO}=\frac{4\pi}{7}M\omega_0^2\{A\langle(r^4)''\rangle+\tfrac{2}{7}(4-K^2)A\langle(r^4P_2)''\rangle + \tfrac{1}{84}[K^2(7K^2-67)+72]A\langle(r^4P_4)''\rangle\}^{-1}, \tag{3.11}$$

with

$$A\langle(r^nP_l)\rangle\equiv\left(\frac{2N}{A}\right)^{2/3}\left\langle\sum_k^N (r_k)^nP_l\right\rangle_0 + \left(\frac{2Z}{A}\right)^{2/3}\left\langle\sum_k^Z (r_k)^nP_l\right\rangle_0. \tag{3.12}$$

A large model space has been used for solving the coupled RPA equations, including seven major shells with $N_{\rm osc}=3$–9 (2–8) for neutrons (protons) in the calculations of positive-parity states, and nine major shells with $N_{\rm osc}=2$–10 (1–9) for the negative-parity states. The mesh of the rotational frequency for the calculations has been chosen as $\Delta\hbar\omega_{\rm rot}=0.01$ MeV which is enough to discuss the properties of band crossing and Coriolis couplings.

Since our mean-field potential is not the simple harmonic oscillator, we use scaling factors f_λ as

$$\chi_{\lambda K}=f_\lambda\chi_{\lambda K}^{\rm HO}, \tag{3.13}$$

for the isoscalar interactions with $\lambda=2$ and 3. These factors are determined by the theoretical and experimental requirements: As for the octupole interactions, we have the experimental Routhians for the lowest octupole vibrational state in SD ^{190}Hg [17]. We assume the common factor f_3 for all K values and fix it so as to reproduce these experimental data. In this case $f_3=1$ can nicely reproduce the experimental Routhians,[3] and we use the same value for ^{192}Hg and ^{194}Hg. For the quadrupole interactions, we determine it so as to reproduce the zero-frequency (Nambu-Goldstone) mode for $K=1$ at $\omega_{\rm rot}=0$ and use the same value for $K=0$ and 2. $f_2=1.007$, 1.005, and 1.005 are obtained for ^{190}Hg, ^{192}Hg, and ^{194}Hg, respectively, by using the adopted model space. The fact that these values of f_λ are close to unity indicates that the size of the adopted model space is large enough.

According to systematic RPA calculations for the low-frequency β, γ, and octupole states in medium-heavy deformed nuclei, we have found that the values of f_λ reproducing the experimental data are very close to unity for the Nambu-Goldstone mode, the γ and octupole vibrational states. On the other hand, those values are quite different from unity for the β vibrational states. This may be associated with the simplicity of the monopole pairing interaction.

[3] This value depends on the treatment of the pairing gaps at finite frequency. If we use constant pairing gaps against $\omega_{\rm rot}$, we get the best value $f_3=1.05$.

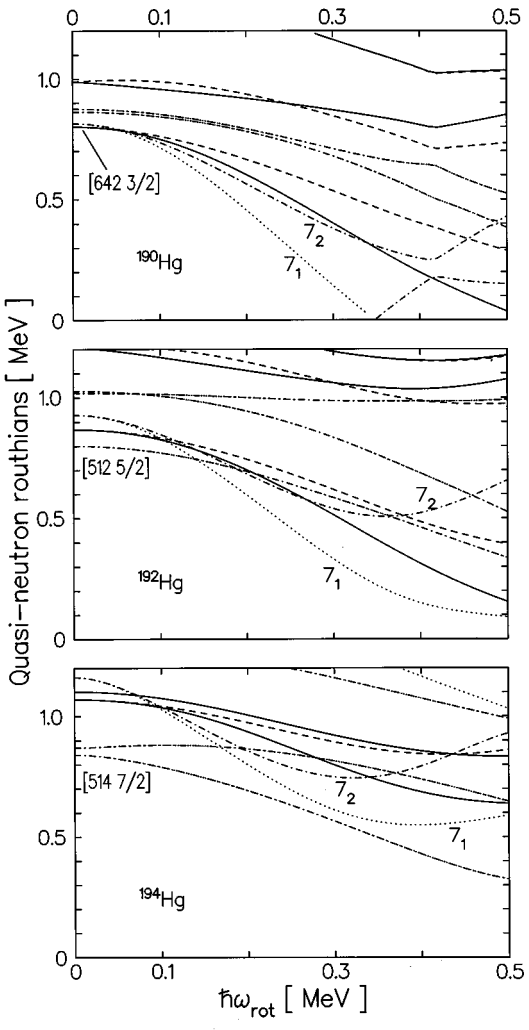

FIG. 3. Neutron quasiparticle Routhians in the Nilsson potential with $h_{\rm add}$ for SD ^{190,192,194}Hg. See text and caption to Fig. 2 for details.

Since we cannot find the realistic force strength χ_{20} for SD states, we do not discuss the property of the β vibrations in this paper.

IV. RESULTS OF NUMERICAL CALCULATIONS

A. Quasiparticle Routhians

In this section we present calculated quasiparticle Routhians in the improved cranked Nilsson potential and discuss their characteristic feature. In Fig. 3 we compare the neutron quasiparticle Routhians for ^{190,192,194}Hg. The proton Routhians of ^{190}Hg are shown above in Fig. 2 and are almost identical for ^{192}Hg and ^{194}Hg.

The calculations show the strong interaction strength between the $\pi([642\ 5/2])^2$ configuration (for simplicity we denote these orbits by $\pi 6_1$ and $\pi 6_2$ in the following) and the yrast configuration which may contribute to the smooth increase of the yrast $\mathcal{J}^{(2)}$ moments of inertia. On the other hand, the interaction of ν [761 3/2] orbits ($\nu 7_1$ and $\nu 7_2$ in the following) strongly depends on the chemical potential (neutron number): The interaction is strongest in ^{194}Hg, and weakest in ^{190}Hg. This is qualitatively consistent with the experimental observation of the yrast $\mathcal{J}^{(2)}$ moments of inertia and the experimental quasiparticle Routhians in ^{191,193}Hg [40,41].

The characteristic features of the high-N intruder orbits are similar to those of the Woods-Saxon potential, except the alignments of $\nu 7_1$ and $\nu 7_2$ orbits which are, respectively, $i \approx 3\hbar$ and $2\hbar$ in ours while $i \approx 4\hbar$ and $3\hbar$ in the Woods-Saxon potential. This results in the different crossing frequency between the ground band and the $\nu(j_{15/2})^2$ band, as discussed in Sec. III A. The observed crossing in ^{190}Hg and the quasiparticle Routhians in ^{191,193}Hg seem to favor our results. There are some other minor differences concerning the position of each orbit in the Nilsson and in the Woods-Saxon potential. However, these differences do not seriously affect our main conclusions because the collective RPA solutions are not sensitive to the details of each orbit.

B. Octupole vibrations

Here, we discuss the negative-parity excitations in SD ^{190,192,194}Hg. We have solved the RPA dispersion equation (2.23) and have obtained all low-lying solutions ($E_x' \leq 2$ MeV). The excitation energies and the $B(E3)$ values calculated at $\omega_{\rm rot}=0$ are listed in Table I. This result shows that $K=2$ octupole states are the lowest for these Hg isotopes, which is consistent with our previous results [3,4]. The $B(E3;0^+ \rightarrow 3^-,K)$ are calculated by using the strong coupling scheme [30] neglecting effects of the Coriolis force. Absolute values of $B(E3)$'s cannot be taken seriously because they depend on the adopted model space and are very sensitive to the octupole coupling strengths χ_{3K}: For instance, if we use $f_3=1.05$ instead of $f_3=1$ in Eq. (3.13), the $B(E3)$ increase by about factor of 2 while the reduction of their excitation energy is about 15%. In addition, the effects of the Coriolis coupling tend to concentrate the $B(E3)$ strengths onto the lowest octupole states [20].

At $\omega_{\rm rot}=0$, the lowest $K=2$ octupole states exhibit almost identical properties in ^{190,192,194}Hg. However, they show different behavior as functions of $\omega_{\rm rot}$ as shown in Figs. 4, 5, and 6, respectively. All RPA solutions, including noncollective solutions as well as collective vibrational ones, are presented in these figures. The size of the circle on the plot indicates the magnitude of the $E3$ transition amplitudes be-

TABLE I. Calculated excitation energies of octupole vibrations and $B(E3;0^+ \rightarrow 3^-,K)$ values estimated using the strong coupling scheme for SD ^{190,192,194}Hg.

	^{190}Hg				^{192}Hg				^{194}Hg			
	$K=0$	$K=1$	$K=2$	$K=3$	$K=0$	$K=1$	$K=2$	$K=3$	$K=0$	$K=1$	$K=2$	$K=3$
E [MeV]	1.37	1.45	1.20	1.52	1.55	1.58	1.18	1.53	1.83	1.62	1.14	1.53
$B(E3)/B(E3)_{\rm s.p.}$	6.6	11.9	10.0	1.0	7.6	10.1	10.1	0.8	11.5	11.2	10.2	0.7

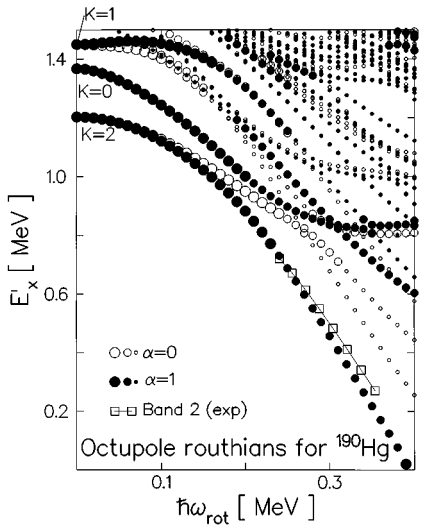

FIG. 4. Calculated RPA eigenenergies of negative-parity states for SD ^{190}Hg, plotted as functions of rotational frequency. Open (solid) circles indicate states with signature $\alpha=0$ ($\alpha=1$). Large, medium, and small circles indicate RPA solutions with $E3$ transition amplitudes $(\Sigma_K|\langle n|Q^e_{3K}|\omega_{\rm rot}\rangle|^2)^{1/2}$ larger than $200e$ fm^3, larger than $100e$ fm^3, and less than $100e$ fm^3, respectively. Note that Routhians for the yrast SD band correspond to the horizontal axis ($E'_x=0$). The observed Routhians for band 2 [17] are shown by open squares.

tween a RPA solution and the yrast state.

The $(K,\alpha)=(2,1)$ octupole state in ^{190}Hg has significant Coriolis mixing and the octupole phonon is aligned along the rotational axis at higher frequency. This is caused by the relatively close energy spacing between the $K=2$ and the $K=0,1$ octupole states in this nucleus. These low-K members of the octupole multiplet are calculated to lie much higher in ^{192}Hg and ^{194}Hg, which reduces the Coriolis mixing in these nuclei. As a result of these phonon alignments, the experimental Routhians for band 2 in ^{190}Hg are nicely reproduced by the lowest $\alpha=1$ octupole state. It should be emphasized that although the excitation energy at one frequency point can be obtained by adjusting the octupole-force

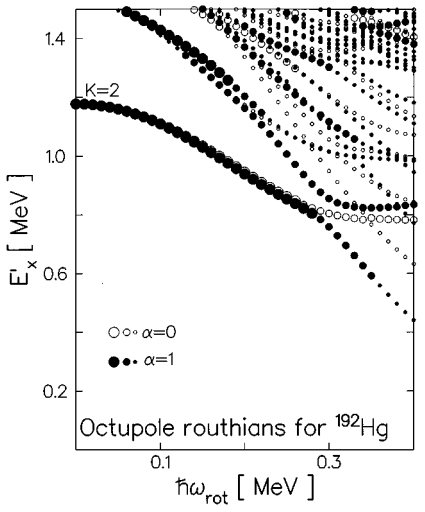

FIG. 5. The same as Fig. 4, but for ^{192}Hg.

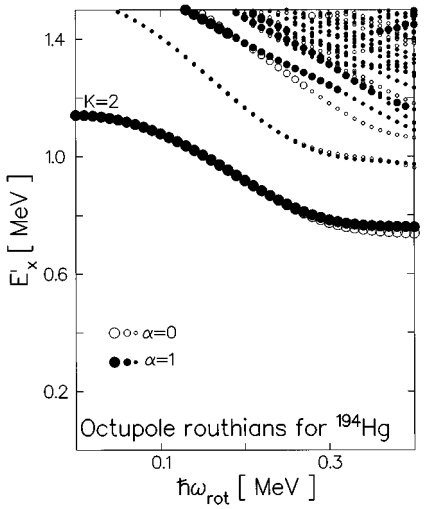

FIG. 6. The same as Fig. 4, but for ^{194}Hg.

strengths, the agreement over the whole frequency region is not trivial.

Since there is no $K=0$ octupole state in the signature $\alpha=0$ sector, the Coriolis mixing is much weaker for the lowest $(K,\alpha)=(2,0)$ octupole state. The calculation predicts that this state is crossed by the negative-parity two-quasiparticle band $\nu(7_1\otimes[642\ 3/2])_{\alpha=0}$ at $\hbar\omega_{\rm rot}\approx 0.27$ MeV.

In ^{192}Hg, the same kind of crossing is seen for both signature partners of the $K=2$ octupole bands. We can clearly see, for the lowest excited state in each signature sector, the transition of the internal structure from collective octupole states (large circles in Fig. 5) to noncollective two-quasineutron states (small circles). The two-quasineutron configurations which cross the octupole vibrational bands are $7_1\otimes[642\ 3/2](\alpha=-1/2)$ for $\alpha=1$ and $7_1\otimes[642\ 3/2](\alpha=1/2)$ for $\alpha=0$. The crossing frequency is lower for the $\alpha=1$ band due to signature splitting of the $\nu[642\ 3/2]$ orbits.

In contrast to ^{190,192}Hg, the $K=2$ octupole bands in ^{194}Hg indicate neither the signature splitting nor the crossings. The Routhians are very smooth up to the highest frequency. This is because the neutron orbits 7_1 and 7_2 have a ''hole'' character and their interaction strengths with the negative-energy orbits become larger with increasing neutron numbers (see Fig. 3). Therefore these orbits go to higher energy and the energies of the two-quasiparticle bands $\nu(7_1\otimes[642\ 3/2])$ never become lower than the $K=2$ octupole bands even at the highest frequency.

These properties of the $K=2$ octupole vibrations come from the effects of the Coriolis force and from the chemical-potential dependence of the aligned two-quasiparticle bands. In order to reproduce these rich properties of the collective vibrations at finite frequency, a microscopic model, which can describe the interplay between the Coriolis force and the correlations of shape fluctuations, is needed.

C. γ vibrations

In this section we present results for the γ-vibrational states built on the SD yrast band. As mentioned in Sec. III B, we do not discuss the property of the β band since it is

TABLE II. Calculated excitation energies of γ vibrations and $B(E2;0^+\rightarrow 2^+,K=2)$ values estimated using the strong coupling scheme for SD ^{190,192,194}Hg.

	^{190}Hg	^{192}Hg	^{194}Hg
E [MeV]	1.39	1.50	1.45
$B(E2)/B(E2)_{\text{s.p.}}$	2.7	3.0	3.8

difficult to determine a reliable value of the coupling strength χ_{20} for the $K=0$ channel of the quadrupole interaction.

The properties of γ bands at $\omega_{\text{rot}}=0$ are listed in Table II. The excitation energies of γ vibrations are predicted to be higher than the $K=2$ octupole vibrations by 200–350 keV. It is known that calculations using the full model space considerably overestimate the $B(E2)$ values. In Ref. [28], it has been shown that the three-N_{osc}-shell calculation reproduces the experimental values very well. If we use the model space $N_{\text{osc}}=5-7$ (4–6) for neutrons (protons), then the $B(E2)$ values in the table decrease by about factor of 1/3. The collectivity of the γ vibrations turns out to be very weak in these SD nuclei.

Figures 7, 8, and 9 illustrate the excitation energy of γ vibrations as functions of the rotational frequency for ^{190}Hg, ^{192}Hg, and ^{194}Hg, respectively. The unperturbed two-quasiparticle Routhians are also depicted by solid (neutrons) and dashed (protons) lines. Since the K quantum number is not a conserved quantity at finite rotational frequency, we have defined the solutions with the large $K=2$ $E2$ transition amplitude as the γ vibrations. As seen in the figure, they lose

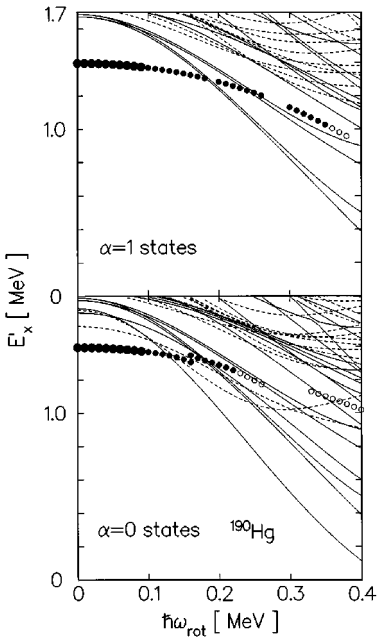

FIG. 7. Calculated RPA eigenenergies for γ vibrational states for SD ^{190}Hg, plotted as functions of rotational frequency. The lower part is for the signature $\alpha=0$ Routhians and the upper for the $\alpha=1$. Large solid, small solid, and small open circles indicate the γ vibrational states whose $K=2$ $E2$ amplitudes $|\langle n|Q^e_{22}|\omega_{\text{rot}}\rangle|$ are larger than $20e$ fm^2, larger than $10e$ fm^2, and less than $10e$ fm^2, respectively. The unperturbed two-quasineutron (two-quasiproton) Routhians are also shown by solid (dashed) lines.

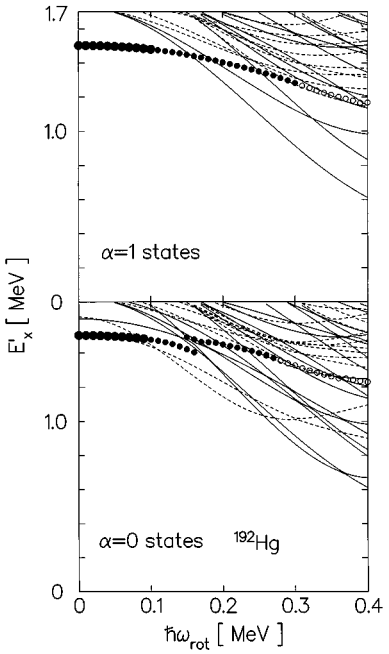

FIG. 8. The same as Fig. 7, but for ^{192}Hg.

their vibrational character by successive crossings with many two-quasiparticle bands and become the dominant two-quasiparticle states at high frequency. The reduction of collectivity is more rapid for the $\alpha=0$ γ vibrations, because the two-quasiparticle states come down more quickly in the $\alpha=0$ sector. Similar crossings occur for the $K=2$ octupole bands in ^{192}Hg (see Fig. 5); however, the crossing frequency is much higher than that of the γ bands. This is because the excitation energies of the octupole bands are relatively lower than those of the γ bands. The predicted properties of γ vibrations are different from those in Ref. [42].

In the frequency region ($0.15\leqslant\hbar\omega_{\text{rot}}\leqslant 0.4$ MeV) where the excited SD bands are observed in experiments, the γ

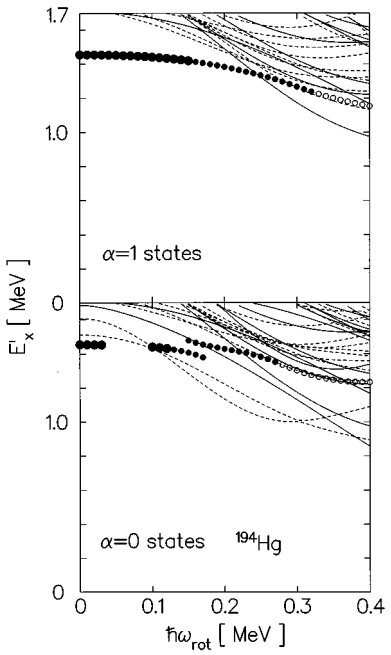

FIG. 9. The same as Fig. 7, but for ^{194}Hg.

TABLE III. The lowest and the second lowest configurations at $\hbar\omega_{\rm rot}=0.4$ MeV in each parity sector. The proposed assignments of the observed excited SD bands are also shown. The excitation energies of the negative-parity two-quasineutron states, 256 keV for ^{190}Hg and 441 and 632 keV for ^{192}Hg, contain very weak octupole correlations. The corresponding unperturbed two-quasineutron energies are 261, 460, and 635 keV, respectively.

		$\pi=+$		$\pi=-$	
		Lowest	Second	Lowest	Second
^{190}Hg	E_x' [keV]	113	389	≈ 0	256
	Config.	$\nu(7_1\otimes 7_2)_{\alpha=0}$	$\nu(7_1\otimes[505\ 11/2])_{\alpha=0,1}$	(oct. vib.)$_{\alpha=1}$	$\nu(7_1\otimes[642\ 3/2])_{\alpha=0}$
	Expt.	Band 3		Band 2	Band 4
^{192}Hg	E_x' [keV]	611	611	441	632
	Config.	$\nu(7_1\otimes[512\ 5/2])_{\alpha=1}$	$\nu(7_1\otimes[512\ 5/2])_{\alpha=0}$	$\nu(7_1\otimes[642\ 3/2])_{\alpha=1}$	$\nu(7_1\otimes[642\ 3/2])_{\alpha=0}$
	Expt.			Band 2	Band 3
^{194}Hg	E_x' [keV]	857	892	738	759
	Config.	$\nu([514\ 7/2])^2_{\alpha=0}$	$\pi([530\ 1/2])^2_{\alpha=0}$	(oct. vib.)$_{\alpha=0}$	(oct. vib.)$_{\alpha=1}$
	Expt.			Band 2	Band 3

bands are predicted to be higher than both the $K=2$ octupole bands and the lowest two-quasiparticle states. Therefore experimental observation of the γ vibrations is expected to be more difficult than that of the octupole bands.

V. COMPARISON WITH EXPERIMENTAL DATA

In this section, we compare the results obtained in the previous section with the available experimental data for the excited SD bands in ^{190,192,194}Hg. The Routhians relative to the yrast SD band have been observed only for band 2 in ^{190}Hg and the comparison with our calculated Routhians has been done in the Sec. IV B. The excitation energies of the other bands are not known. Therefore, in order to compare our theory with experimental data, we have calculated the dynamic moments of inertia, $\mathcal{J}^{(2)}$.

It is known that the effects of $N_{\rm osc}$ mixing, pairing fluctuations, and higher-multipole pairing are important in reproducing absolute magnitude of the moments of inertia. On the other hand, our model aims at describing relative quantities (excitation energy, alignment, etc.) between the excited and yrast bands. Thus, instead of directly calculating $\mathcal{J}^{(2)}$ in terms of Eq. (2.10), we decompose the $\mathcal{J}^{(2)}$ of the excited bands as

$$\mathcal{J}^{(2)}(\omega)=\mathcal{J}_0^{(2)}(\omega)+\frac{di}{d\omega}=\mathcal{J}_0^{(2)}(\omega)-\frac{d^2E_x'}{d\omega^2}, \quad (5.1)$$

where $\mathcal{J}_0^{(2)}$ denotes the dynamic moments of inertia for the yrast SD bands (RPA vacuum), and i and E_x' are the calculated alignments and Routhians relative to the yrast band, respectively. The $\mathcal{J}_0^{(2)}$ values of the yrast SD bands are taken from the experiments and approximated by the Harris expansion,

$$\mathcal{J}_0^{(2)}(\omega)=J_0+3J_1\omega^2+5J_2\omega^4. \quad (5.2)$$

The expression (5.1) phenomenologically takes account of the effects mentioned above. Those effects are included in the experimental $\mathcal{J}_0^{(2)}$ of Eq. (5.2).

The lower the excitation energy of an excited band relative to the yrast SD band, the more strongly will it be populated. In experiments, the SD bands are populated at high frequency; thus, it is the excitation energy in the feeding region at high frequency that is relevant in this problem. We list in Table III the calculated excitation energies of the low-lying positive- and negative-parity states at $\hbar\omega_{\rm rot}=0.4$ MeV.

In ^{190}Hg three excited SD bands (bands 2, 3, and 4) have been observed [16–18]. Band 2 has been assigned as the lowest octupole band [16,17] because of its strong decays into the yrast SD band. According to our calculations, in addition to this octupole band ($\alpha=1$), the aligned two-quasineutron bands come down at high frequency. We assign band 4 at high frequency as the $\nu(7_1\otimes[642\ 3/2])_{\alpha=0}$ because this negative-parity two-quasineutron state is crossed by the $\alpha=0$ octupole band at $\hbar\omega_{\rm rot}\approx 0.26$ MeV which may correspond to the observed sharp rise of $\mathcal{J}^{(2)}$ at $\hbar\omega_{\rm rot}\approx 0.23$ MeV (Fig. 4). The positive-parity $\nu(7_1\otimes 7_2)_{\alpha=0}$ state is also relatively low lying at high frequency. Since this band does not show any crossing at $\hbar\omega_{\rm rot}>0.12$ MeV in the calculations, this may be a good candidate for band 3 (Fig. 7).

In ^{192}Hg, two excited SD bands (bands 2 and 3) have been observed [22] and both bands exhibit a bump in $\mathcal{J}^{(2)}$ at $\hbar\omega_{\rm rot}\approx 0.3$ MeV (band 2) and 0.33 MeV (band 3). We assume these bands correspond to $\nu(7_1\otimes[642\ 3/2])_{\alpha=0,1}$ at high frequency. This two-quasineutron configuration for band 2 is the same as that suggested in Ref. [22]. However, our theory predicts a different scenario at low spin: This band is crossed by the octupole band ($\alpha=1$) at $\hbar\omega_{\rm rot}\approx 0.3$ MeV. Thus, band 2 is interpreted as an $\alpha=1$ octupole vibrational band in the low-frequency region ($\hbar\omega_{\rm rot}<0.3$ MeV). In the same way, the bump in $\mathcal{J}^{(2)}$ in band 3 is interpreted as a crossing between $\nu(7_1\otimes[642\ 3/2])_{\alpha=0}$ and the $\alpha=0$ octupole vibrational band (Fig. 5).

For high frequencies, the positive-parity $\nu(7_1\otimes[512\ 5/2])$ state is calculated to lie almost at the same energy as the lowest $\alpha=0$ negative-parity state. However, no crossing is predicted for the $\alpha=1$ state at

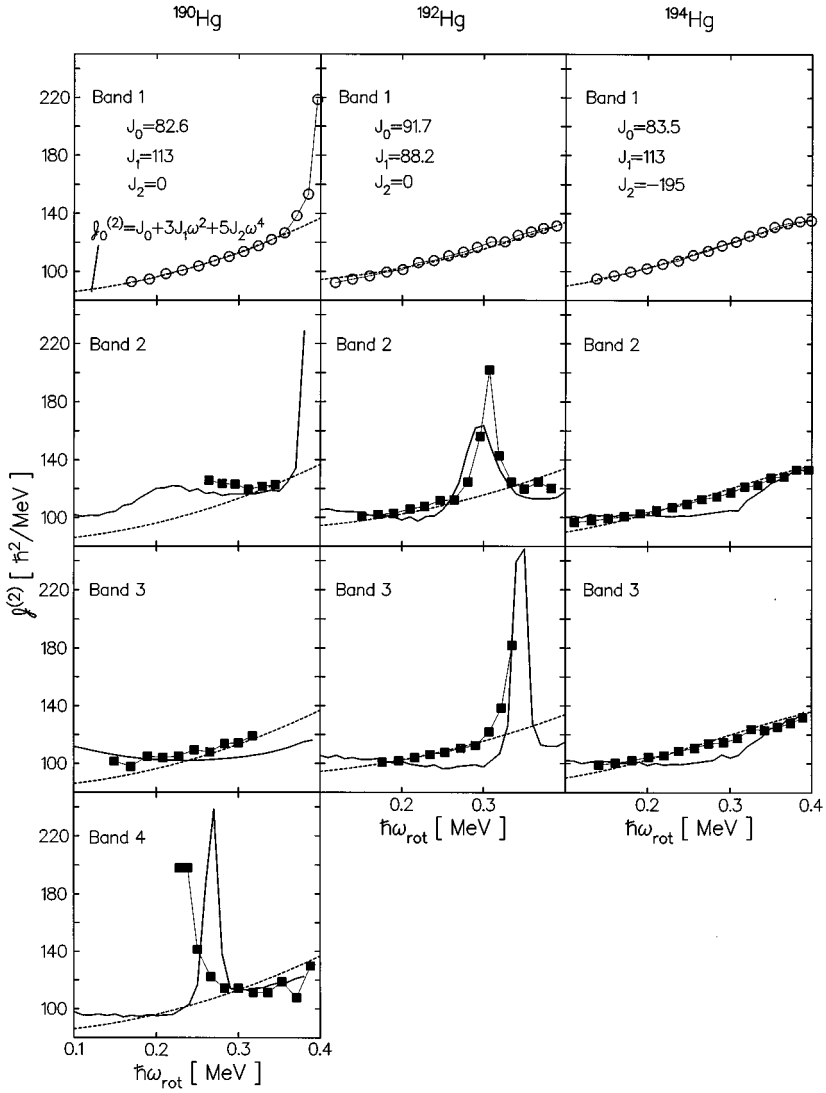

FIG. 10. Calculated (solid lines) and experimental (symbols) dynamic moments of inertia for excited SD bands in ^{190}Hg (left), ^{192}Hg (middle), and ^{194}Hg (right). $\mathcal{J}^{(2)}$ for the yrast SD bands are also displayed at the top. Dotted lines indicate the yrast $\mathcal{J}^{(2)}$, which are approximated by the Harris formula (5.2). The parameters J_0, J_1, and J_2 used in the formula are shown in units of $\hbar^2$ MeV^{-1}, $\hbar^4$ MeV^{-3}, and $\hbar^6$ MeV^{-5}, respectively.

$\hbar\omega_{\rm rot}>0.15$ MeV but many crossings are predicted for the $\alpha=0$ state (Fig. 8). Both properties are incompatible with the observed features.

In ^{194}Hg, two excited SD bands (bands 2 and 3) have been observed [23,24]. In contrast to ^{192}Hg, the observed dynamic moments of inertia, $\mathcal{J}^{(2)}$, do not show any singular behavior and are more or less similar to those of the yrast band. Bands 2 and 3 have been interpreted as signature partners because the γ-ray energies of band 3 are observed to lie midway between those of band 2 and furthermore the bands have similar intensity [23]. From these observations and the excitation energies listed in Table III, we assume that both bands correspond to $K=2$ octupole vibrations ($\alpha=0$, 1), which are calculated to be the lowest excited states (Fig. 6). Any other assignment faces serious difficulties: (i) The positive-parity two-quasiparticle configurations listed in Table III have no signature partners. (ii) The other low-lying two-quasiparticle states occupy $\nu 7_1$ or $\pi 6_1$ orbits. Now the increase in $\mathcal{J}^{(2)}$ for the yrast SD band is partially attributed to the alignment of these high-j intruder orbits and, since the blocking effect of the quasiparticles prevents any alignment due to band crossings involving these orbits, the lack of alignment should produce an $\mathcal{J}^{(2)}$ curve quite different from those of the yrast SD band. (iii) The configuration $\nu([512\ 5/2]\otimes[624\ 9/2])$ suggested in Ref. [23] has a problem with its magnetic property, which has been recently pointed out in Ref. [43]. If this configuration is the $K^\pi=7^-$, then strong $M1$ transitions between the signature partners should have been observed. The energy of the $K^\pi=2^-$ configuration is certainly lowered by octupole correlations. In our calculations, however, this configuration accounts for only 20% of all components constituting the octupole vibration (iv). The γ vibrations are calculated to be much higher and crossed by several two-quasiparticle bands (Fig. 9). Therefore, we believe the octupole vibration is the best candidate.[4]

Assuming the above configurations, the dynamic moments of inertia, $\mathcal{J}^{(2)}$, are calculated with Eq. (5.1), and compared with the experimental data (Fig. 10). In ^{190}Hg, the characteristic features are well reproduced for bands 2 and 4; the constant $\mathcal{J}^{(2)}$ of band 2 (the $\alpha=1$ octupole vibration) and the bump of band 4 (the crossing between the $\alpha=0$

[4]The signature for bands 2 and 3 is determined by following the spin assignment in Ref. [23].

octupole vibration and the aligned two-quasineutron band) are reproduced although the crossing frequency is smaller in the experiment. For band 3, the high $\mathcal{J}^{(2)}$ values at low spin are well accounted for by the alignment gain of the two-quasineutron state. However, the calculation predicts the lack of alignment due to the blocking of $N=7$ orbits at $\hbar\omega_{\rm rot}>0.25$ MeV, which makes the $\mathcal{J}^{(2)}$ smaller than those of the yrast band.

In ^{192}Hg, the bumps of $\mathcal{J}^{(2)}$ are nicely reproduced in the calculations, which correspond to the crossings between $K=2$ octupole vibrations and the aligned two-quasineutron bands in each signature partner. The alignment gain Δi before and after crossing for band 2 is $\Delta i\approx 2\hbar$ which is comparable to the experimental value $\Delta i_{\rm expt}\approx 2.6\hbar$ [22].

The agreement is less satisfactory in ^{194}Hg. The calculated $\mathcal{J}^{(2)}$ are lower than the experimental data for $0.2\leqslant\hbar\omega_{\rm rot}\leqslant 0.35$ MeV (similar disagreement can be seen for band 3 in ^{192}Hg). This effect comes from the blocking effect mentioned above, associated with the $\nu 7_1$, $\nu 7_2$, $\pi 6_1$, and $\pi 6_2$ orbits. In the RPA (Tamm-Dancoff) theory (neglecting the backward amplitudes), the octupole vibrations are described by superposition of two-quasiparticle excitations,

$$|\text{oct vib}\rangle=\sum_{\gamma\delta}\psi(\gamma\delta)|\gamma\delta\rangle, \tag{5.3}$$

where $|\gamma\delta\rangle=a^\dagger_\gamma a^\dagger_\delta|\omega_{\rm rot}\rangle$. Some of these components $|\gamma\delta\rangle$ associated with the particular orbits ($\nu 7_1$, $\nu 7_2$, $\pi 6_1$, and $\pi 6_2$) show significant lack of alignment. However, if the octupole vibrations are collective enough, the amplitudes $\psi(\gamma\delta)$ are distributed over many two-quasiparticle excitations $|\gamma\delta\rangle$. Thus, each amplitude becomes small and blocking effects may be canceled.

In order to demonstrate this ''smearing'' effect of collective states, we use a slightly stronger octupole force, $f_3=1.05$ in Eq. (3.13), and carry out the same calculations for ^{194}Hg. The results are shown in Fig. 11. The higher coupling strengths make the octupole vibrations more collective and the experimental data are better reproduced. Perhaps the collectivity of these octupole vibrations was underestimated in the calculations with $f_3=1$.

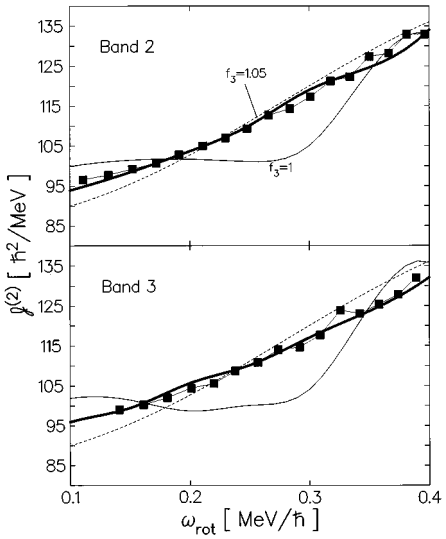

FIG. 11. Calculated (solid lines) and experimental (symbols) dynamic moments of inertia for excited SD bands in ^{194}Hg. Thin solid lines are the same as in Fig. 10, while thick lines indicate the results obtained by using the slightly stronger coupling strengths ($f_3=1.05$) for the octupole interactions. Dotted lines indicate the $\mathcal{J}^{(2)}$ for the yrast SD band (see caption to Fig. 10).

Finally we should mention the decays from the octupole bands to the yrast SD band. We have assigned all observed excited SD bands (except band 3 in ^{190}Hg) as octupole vibrational bands (at least in the low-spin region). However, strong dipole decays into the yrast band have been observed only for band 2 in ^{190}Hg. Although this seems to contradict our proposals, in fact our calculations provide us with a qualitative answer.

Let us discuss the relative $B(E1;\text{oct}\rightarrow\text{yrast})$ values. Using the $E1$ recoil charge ($-Ze/A$ for neutrons and Ne/A for protons), then the $B(E1)$ values at $\hbar\omega_{\rm rot}=0.25$ MeV are calculated to be small for all the $K=2$ octupole bands except

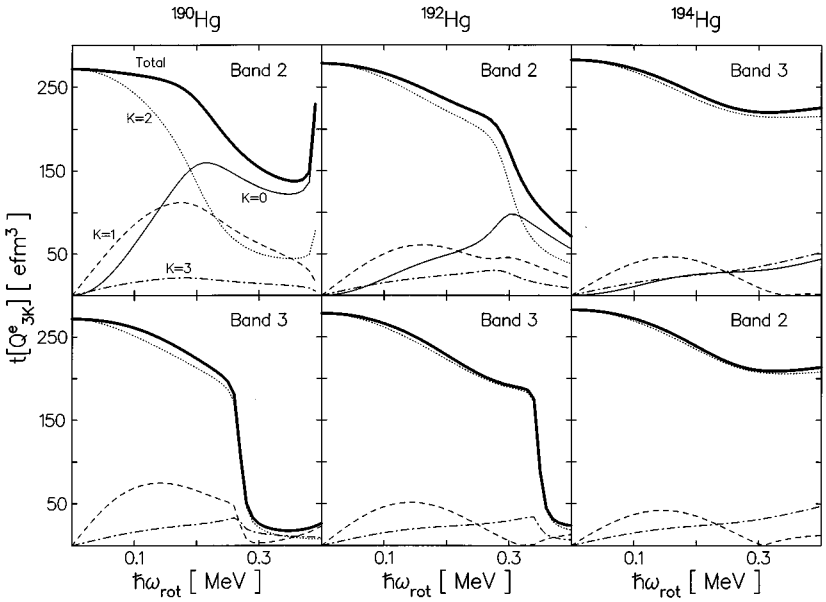

FIG. 12. Electric $E3$ transition amplitudes, $|t[1/2(1+\tau_3)Q^\alpha_{3K}]|=|\langle\omega_{\rm rot}|Q^e_{3K}|n\rangle|$, for the lowest RPA solutions with the signature $\alpha=0$ (lower) and the $\alpha=1$ (upper) for ^{190}Hg (left), ^{192}Hg (middle), and ^{194}Hg (right). $K=0$, 1, 2, and 3 components are denoted by solid, dashed, dotted, and dash-dotted lines, respectively. Total values (thick solid lines) are defined by $(\Sigma_K|\langle\omega_{\rm rot}|Q^e_{3K}|n\rangle|^2)^{1/2}$.

for the $\alpha=1$ (band 2) in ^{190}Hg: With the scaling factors $f_3=1\sim1.08$ in Eq. (3.13), the calculation suggests $B(E1)\approx10^{-7}$ Weisskopf units (W.u.) for the $(K,\alpha)=(2,0)$ octupole bands, and $B(E1)\approx10^{-8}$–10^{-6} W.u. for the $(K,\alpha)=(2,1)$ bands. The $B(E1)$ for band 2 in ^{190}Hg is predicted to be larger than these values by one to two orders of magnitude, $B(E1)\approx10^{-6}$–10^{-4} W.u. Although the absolute values are very sensitive to the parameters used in the calculation, the $E1$ strengths of band 2 in ^{190}Hg are always much larger than those for the other bands.

To clarify the reason for this $E1$ enhancement in this particular band, we display the $E3$ amplitudes ($K=0$, 1, 2, and 3) of these octupole states as functions of frequency in Fig. 12. As mentioned in Sec. IV B, the Coriolis mixing is completely different between band 2 in ^{190}Hg and the others: The former has significant Coriolis mixing at finite frequency while the latter retains the dominant $K=2$ character up to very high spin. Since the $K=2$ octupole components cannot carry any $E1$ strength, the strong $E1$ transition amplitudes come from Coriolis coupling, namely, the mixing of the $K=0$ and 1 octupole components. Therefore, the observed decay property does not contradict our interpretation.

VI. CONCLUSIONS

The microscopic structure of the γ and the octupole vibrations built on the SD yrast bands in ^{190,192,194}Hg were investigated with the RPA based on the cranked shell model. The $K=2$ octupole vibrations are predicted to lie lowest. To reproduce the characteristic features of the experimental data it was essential to include octupole correlations and the effect of rapid rotation explicitly. From the calculations, we assigned the following configurations to the observed excited bands:

^{190}Hg	Band 2:	The rotationally aligned $\alpha=1$ octupole vibration.
	Band 3:	the two-quasineutron band $\nu(7_1\otimes7_2)$.
	Band 4:	the $(K,\alpha)=(2,0)$ octupole vibration at low spin, the two-quasineutron band $\nu(7_1\otimes[642\ 3/2])_{\alpha=0}$ at high spin.
^{192}Hg	Band 2:	the $(K,\alpha)=(2,1)$ octupole vibration at low spin, the two-quasineutron band $\nu(7_1\otimes[642\ 3/2])_{\alpha=1}$ at high spin.
	Band 3:	the $(K,\alpha)=(2,0)$ octupole vibration at low spin, the two-quasineutron band $\nu(7_1\otimes[642\ 3/2])_{\alpha=0}$ at high spin.
^{194}Hg	Band 2:	the $(K,\alpha)=(2,0)$ octupole vibration.
	Band 3:	the $(K,\alpha)=(2,1)$ octupole vibration.

With these assignments, most of the experimentally observed features were well accounted for in our theoretical calculations.

The Coriolis force makes the lowest octupole state in ^{190}Hg align along the rotational axis, while this effect is predicted to be very weak for other octupole states. This is due to the relatively low excitation energy of the $K=0$ ($\alpha=1$) octupole state in ^{190}Hg, in which the close spacing in energy of the octupole multiplet makes the Coriolis mixing easier. This aligned octupole phonon in ^{190}Hg reproduces the observed behavior for band 2.

Our interpretation for the excited SD bands in ^{192}Hg solves a puzzle mentioned in Ref. [22] in which band 2 was assigned as the two-quasineutron excitation $\nu(7_3\otimes[642\ 3/2])$. The bump in the $\mathcal{J}^{(2)}$ curve was considered to be associated with a crossing between the $\nu7_1$ and ν [512 5/2] orbits. According to this assignment, we expect similar properties for the observed crossing in ^{192}Hg and ^{193}Hg, and the difference of crossing frequencies and alignment gains was a puzzle. This is no longer a puzzle in our interpretation because the microscopic structure of band 2 is the octupole vibration (before the crossing). Because of the correlation-energy gains, the excitation energies of the octupole vibrations should be lower than the unperturbed two-quasiparticle states. Therefore it is natural that the observed crossing frequency is larger than the one predicted by the quasiparticle Routhians without the octupole correlations.

Our interpretation also solves some difficulties in ^{194}Hg: The smooth $\mathcal{J}^{(2)}$ behavior of bands 2 and 3 can be explained by the ''smearing'' effect of the collective states. The nonobservation of the expected strong $M1$ transitions between bands 2 and 3 [43] is solved by substituting the $K=2$ octupole vibrations for the two-quasineutron states $\nu([512\ 5/2]\otimes[624\ 9/2])$, because the octupole correlations lower the $K=2$ configurations and the summation of many two-quasiparticle ($M1$) matrix elements may be destructive [see discussion below Eq. (2.26)].

Enhanced $E1$ transitions from the octupole states to the yrast SD band are expected only for band 2 in ^{190}Hg. This comes about because the other octupole states do not have strong Coriolis mixing and keep their $K=2$ character even at high frequency. This agrees with experimental observations.

Although most of the observed properties are explained by our calculations, there remain some unsolved problems in ^{190}Hg and ^{192}Hg. For ^{190}Hg, according to the calculations with constant pairing gaps reported in Ref. [19], it is suggested that band 4 may correspond to the $(K,\alpha)=(1,0)$ octupole band which is predicted to be crossed by the two-quasineutron band $\nu(7_1\otimes[642\ 3/2])_{\alpha=0}$ at $\hbar\omega_{\rm rot}\approx0.21$ MeV. Because of the phenomenological treatment for the pairing gaps at finite frequency, it is difficult to deny this possibility. The experimental intensity of band 3 raises another ambiguity: Since it is much weaker than bands 2 and 4, it might be associated with a higher-lying configurations [18]. For ^{192}Hg, our calculations predict no signature splitting for the lowest octupole bands at $\hbar\omega_{\rm rot}\leqslant0.25$ MeV. Therefore one may expect γ-ray energies typical of the signature-partner pair for bands 2 and 3 similar to that in ^{194}Hg, which is different from what is observed [22]. Improvement of the pairing interactions (fluctuations, quadrupole pairing) might solve these problems as well as enable us to perform reliable RPA calculations for β vibrations.

Theoretical study of octupole vibrations carrying large $E1$ strengths would be of great interest, because this could offer direct experimental evidence. An improved version of

calculations for $E1$ strengths of high-spin octupole bands is in progress, taking into account the restoration of translational and Galilean invariance. The $K=0$ octupole vibration in ^{152}Dy has been predicted in Ref. [5] and its decay into the yrast band has been suggested [14]. Strong $E1$ transition probabilities have been suggested by Skalski [44] for $K=0$ octupole states in the $A=190$ region. Therefore, the search for low-lying low-K octupole vibrations is an important subject for the future.

ACKNOWLEDGMENTS

We would like to acknowledge W. Nazarewicz for discussions and suggestions for this paper. One of authors (T.N.) also thanks B. Crowell, P. Fallon, J.F. Sharpey-Schafer, J. Skalski, and A.N. Wilson for valuable discussions. Three of us (T.N., K.M., and Y.R.S.) thank the Institute for Nuclear Theory at the University of Washington for its hospitality and the U.S. Department of Energy for partial support during the completion of this work.

[1] S. Mizutori, Y.R. Shimizu, and K. Matsuyanagi, Prog. Theor. Phys. **83**, 666 (1990); **85**, 559 (1991); **86**, 131 (1991).

[2] T. Nakatsukasa, S. Mizutori, and K. Matsuyanagi, Prog. Theor. Phys. **87**, 607 (1992).

[3] T. Nakatsukasa, S. Mizutori, and K. Matsuyanagi, Prog. Theor. Phys. **89**, 847 (1993).

[4] S. Mizutori, T. Nakatsukasa, K. Arita, Y.R. Shimizu, and K. Matsuyanagi, Nucl. Phys. **A557**, 125c (1993).

[5] T. Nakatsukasa, K. Matsuyanagi, S. Mizutori, and W. Nazarewicz, Phys. Lett. B **343**, 19 (1995).

[6] J. Dudek, T.R. Werner, and Z. Szymański, Phys. Lett. B **248**, 235 (1990).

[7] S. Åberg, Nucl. Phys. **A520**, 35c (1990).

[8] J. Höller and S. Åberg, Z. Phys. A **336**, 363 (1990).

[9] P. Bonche, S.J. Krieger, M.S. Weiss, J. Dobaczewski, H. Flocard, and P.-H. Heenen, Phys. Rev. Lett. **66**, 876 (1991).

[10] Xunjun Li, J. Dudek, and P. Romain, Phys. Lett. B **271**, 281 (1991).

[11] W. Nazarewicz and J. Dobaczewski, Phys. Rev. Lett. **68**, 154 (1992).

[12] J. Skalski, Phys. Lett. B **274**, 1 (1992).

[13] J. Skalski, P.-H. Heenen, P. Bonche, H. Flocard, and J. Meyer, Nucl. Phys. **A551**, 109 (1993).

[14] P.J. Dagnall *et al.*, Phys. Lett. B **335**, 313 (1995).

[15] D.M. Cullen *et al.*, Phys. Rev. Lett. **65**, 1547 (1990).

[16] B. Crowell *et al.*, Phys. Lett. B **333**, 320 (1994).

[17] B. Crowell *et al.*, Phys. Rev. C **51**, R1599 (1995).

[18] A.N. Wilson *et al.*, in *Low Energy Nuclear Dynamics (LEND'95)*, Proceedings of European Physical Society XV Nuclear Physics Divisional Conference, St Petersburg, Russia, 1995 (World Scientific, Singapore, 1995), p. 545.

[19] T. Nakatsukasa, Act. Phys. Pol. B **27**, 59 (1996).

[20] K. Neergård and P. Vogel, Nucl. Phys. **A145**, 33 (1970); **A149**, 209 (1970); **A149**, 217 (1970).

[21] P. Vogel, Phys. Lett. **66B**, 431 (1976).

[22] P. Fallon *et al.*, Phys. Rev. C **51**, R1609 (1995).

[23] M.A. Riley *et al.*, Nucl. Phys. **A512**, 178 (1990).

[24] B. Cederwall *et al.*, Phys. Rev. Lett. **72**, 3150 (1995).

[25] E.R. Marshalek, Phys. Rev. C **11**, 1426 (1975); Nucl. Phys. **A266**, 317 (1976).

[26] J.L. Egido, H.J. Mang, and P. Ring, Nucl. Phys. **A339**, 390 (1980).

[27] Y.R. Shimizu and K. Matsuyanagi, Prog. Theor. Phys. **79**, 144 (1983); **72**, 799 (1984).

[28] Y.R. Shimizu and K. Matsuzaki, Nucl. Phys. **A588**, 559 (1995).

[29] I.M. Robledo, J.L. Egido, and P. Ring, Nucl. Phys. **A449**, 201 (1986).

[30] A. Bohr and B.R. Mottelson, *Nuclear Structure* (Benjamin, New York, 1975), Vol. 2.

[31] S. Kinouchi, Ph.D. thesis, University of Tsukuba, 1988.

[32] Y.R. Shimizu, E. Vigezzi, and R.A. Broglia, Nucl. Phys. **A509**, 80 (1990).

[33] H. Sakamoto and T. Kishimoto, Nucl. Phys. **A501**, 205 (1989).

[34] T. Bengtsson and I. Ragnarsson, Nucl. Phys. **A436**, 14 (1985).

[35] M. Baranger and K. Kumar, Nucl. Phys. **A110**, 490 (1968).

[36] M. Brack, J. Damgaard, A.S. Jensen, H.C. Pauli, V.M. Strutinsky, and C.Y. Wong, Rev. Mod. Phys. **44**, 320 (1972).

[37] R. Wyss, W. Satula, W. Nazarewicz, and A. Johnson, Nucl. Phys. **A511**, 324 (1990).

[38] M.W. Drigert *et al.*, Nucl. Phys. **A530**, 452 (1991).

[39] H. Sakamoto, Nucl. Phys. **A557**, 583c (1993).

[40] M.J. Joyce *et al.*, Phys. Lett. B **340**, 150 (1994).

[41] M.P. Carpenter *et al.*, Phys. Rev. C **51**, 2400 (1995).

[42] M. Girod, J.P. Delaroche, J. Libert, and I. Deloncle, Phys. Rev. C **45**, R1420 (1992).

[43] P.B. Semmes, I. Ragnarsson, and S. Åberg, Phys. Lett. B **345**, 185 (1995).

[44] J. Skalski, Phys. Rev. C **49**, 2011 (1994).